Journal of Cluster Science (2021) 32:1299–1309
https://doi.org/10.1007/s10876-020-01894-5

ORIGINAL PAPER

Biogenic Synthesis of Silver Nanoparticles Using *Streptomyces* spp. and their Antifungal Activity Against *Fusarium verticillioides*

Kiran Marathe[1] · Jitendra Naik[1] · Vijay Maheshwari[2]

Received: 8 May 2020 / Accepted: 13 September 2020 / Published online: 29 September 2020

Abstract

The present study reports the synthesis of silver nanoparticles (AgNPs) using haloalkaliphilic *Streptomyces* spp. characterization, and antifungal activity thereof. The UV visible spectra of synthesized AgNPs showed a characteristic absorption peak at 430 nm, due to the excitation of Surface Plasmon Resonance. Scanning electron microscopy and transmission electron microscopy images showed spherical shape NPs with an average particle size of 16.4 ± 2.2 nm. The crystalline structure of the AgNPs was confirmed by X-ray diffraction (XRD). Zeta potential analyses revealed that NPs were negatively charged (− 8.12 ± 3.87 mV). The synthesized AgNPs are significantly active against phytopathogenic fungi, *Fusarium verticillioides* and *Ustilago maydis*. Microscopic, histo- and bio-chemical investigation of AgNPs against *F. verticillioides* revealed that AgNPs at 100 µg concentration inhibits the hyphal growth and conidia germination, and ∼ 42.85% reduction of ergosterol biosynthesis. The results of propidium iodide staining and high relative cell membrane conductivity confirmed AgNPs mediated damage to the membrane. Moreover, the AgNPs synthesized by *Streptomyces* spp. inhibit the growth of *F. verticillioides* could be due to the inhibition of ergosterol biosynthesis and membrane damage. In our knowledge, this is the first report demonstrating the anti *F. verticillioides* activity of AgNPs synthesized by *Streptomyces* spp.

Keywords *F. verticillioides* · *Streptomyces* spp · Ergosterol · Silver nanoparticles

Introduction

Nanotechnology is a promising field of science which deals with the synthesis and development of different nano-sized (10–100 nm) structures [1]. Nowadays, the synthesis of nanoparticles attracted much more attention due to their large surface-to-volume ratio, which render them highly useful in the fields of medical, electronic, and material science [2]. So far, nanoparticles of silica, selenium, copper, magnesium, gold, and silver have been reported in the field of biomedicine [3, 4], biosensor technology [5], catalytic reduction [6], and bioremediation [7, 8] respectively. Of these nanoparticles, most studied are silver nanoparticles (AgNPs) due to their potential applications in multiple fields [9]. Besides this, AgNPs are found to be excellent antibacterial, antifungal, and anti-inflammatory agents [9, 10]. Considering biomedical importance, biogenic, non-toxic, safe, and eco-friendly synthesis of AgNPs has been in focus and extracts of medicinal plants, cell mass or culture filtrate of microorganisms, fungi, and algae were investigated for this purpose [11–13].

Actinomycetes are filamentous soil bacteria with a morphologically complex life cycle. They are a prolific producer of a variety of antibiotics/bioactive and enzymes during growth [13, 14]. As per the literature survey, 75% of antibiotics have been isolated from *Streptomyces* spp. Therefore, the potential of *Streptomyces* spp. isolated from different habitats is explored by many researchers for the reduction of silver ions, thereby the synthesis of controlled size silver nanoparticles [13, 15–18]. But there are no reports on haloalkaliphilic salt-tolerant *actinobacteria* mediated synthesis of silver nanoparticles.

✉ Kiran Marathe
marathekiran23@gmail.com

[1] University Institute of Chemical Technology, Kavayitri Bahinabai Chaudhari North Maharashtra University, Jalgaon, MS 425001, India

[2] School of Life Sciences, Kavayitri Bahinabai Chaudhari North Maharashtra University, Jalgaon, MS 425001, India

Various plant diseases caused by fungi lead to substantial losses in crops like rice, barley, wheat, grapevine, cotton, groundnut etc. [19, 20]. Besides this, they cause a potential adverse effects on human health by producing toxic secondary metabolites such as fumonisin B1, zearalenone, deoxynivalenol, moniliformin [21]. The mycotoxins are mostly produced by genera of phytopathogenic fungi viz. *Aspergillus* spp., *Fusarium* spp., and *Penicillium* spp. [21]. Among these, *Fusarium* spp. are widely distributed and grow on a variety of plant hosts. Particularly, *F. verticillioides* (previously known as *F. moniliforme*) infects the maize seeds both on the field and post-harvesting [22]. The complete irradiation of *F. verticillioides* contamination is difficult due to the unavailability of proper fungicide treatment [22] and this affects the crop yield and human health. Synthetic/chemical fungicides are reported to control such infections but due to their detrimental effects on human health, they have limited scope. Therefore, there is a necessity to look for alternative eco-friendly and safe bio-fungicide to control the fungal phytopathogen.

Antimicrobial potential of silver nanoparticles against various types of bacteria has been reported [23], however, few reports showed antifungal potential [24–26]. To the best of our knowledge, there is no report on haloalkaliphilic *Streptomyces* mediated synthesis of silver nanoparticles to control *F. verticillioides.* On this premise, the present study describes the synthesis, characterization of AgNPs from previously isolated *Streptomyces* spp. [27, 28] and evaluation of the antifungal potential of AgNPs and their mechanism of action against the mycotoxigenic fungal phytopathogen *Fusarium verticillioides.*

Materials and Methods

All analytical grade chemicals were procured from Sigma Aldrich (St Louis, USA). Potato dextrose agar (PDA) was purchased from HiMedia (Mumbai, India). The plant pathogenic fungi such as *Fusarium verticillioides* (previously known as *F. moniliforme*) (NCIM 1099), *Rhizoctonia solani* (NCIM 1348), *Ustilago maydis* (NCIM 983), *Sclerotinia sclerotiorum* (NCIM 8785), *Colletotrichum dematium* (MTCC 10538), and *Colletotrichum circinans* (MTCC 10329) were obtained from National Collection of Industrial Microorganisms (NCIM), Pune and Microbial Type Culture Collection (MTCC), Chandigarh, India. The *Streptomyces* strains VL 5, VL 18, VL 50 and VL J2 were previously isolated and maintained in the laboratory.

Screening of *Streptomyces* spp. for the biological synthesis of silver nanoparticles (AgNPs)

The *Streptomyces* strains (VL 5, VL 18, VL 50 and VL J2) were each cultivated separately in 100 mL of starch casein broth (pH 8.5) on an orbital shaker (120 rpm) at 30 °C for 48 h [28]. The cell pellets were collected by centrifugation at $5000\times g$ for 10 min and washed twice with distilled water. The 1.0% (w/v) biomass of each strain was inoculated separately into 100 mL MGYP medium [comprising (gL^{-1}): malt extract 3; glucose, 10; yeast extract, 3 and peptone, 5] and incubated for 48 h as described above. After incubation, the supernatant of each strain was collected by centrifugation at $5000\times g$ for 10 min and used separately for the synthesis of AgNPs as previously described [18]. In brief, 5 mL of culture supernatant was mixed with 50 ml $AgNO_3$ (1 mM) and incubated at 28 °C for 48 h on orbital shaker (200 rpm). The color change (yellow to dark brown) was monitored using UV–visible spectroscopy (UV 1800, Shimadzu, Japan). The $AgNO_3$ solution with MGYP medium (without *Streptomyces* spp.) served as a control. The NPs were collected by centrifugation at $10{,}000\times g$ for 30 min, and dried at 40 °C in hot air oven.

Characterization of AgNPs

Spectrophotometric Analysis

The spectrophotometric analysis was performed using UV 1800, UV–visible spectrophotometer (Shimadzu, Japan). The samples were scanned between 700 to 300 nm for the detection of the characteristic absorption peak at 430 nm.

Scanning and Transmission Electron Microscopy

The dried NPs were applied on carbon taped and imaged using field emission scanning electron microscope (FESEM, S-4800, Hitachi, Japan). The elemental silver analysis was performed by using energy-dispersive x-ray (EDX) detector (Bruker, Germany). High resolution-transmission electron microscopy (HR-TEM) images were obtained by using a FEI, TecnaiG2, F 30-TEM. The selected area electron diffraction (SAED) pattern was collected for the NPs applied on carbon-coated copper TEM grids. The size of the NPs was analyzed using ImageJ software (Scion Corporation, USA) [23].

X-ray Diffraction (XRD) Analysis

The crystallinity and particle size of AgNPs were determined by X' Pert Pro XRD (X'Pert^3 Powder, Malvern,

UK) equipped with x′ Celerator solid-state detector. The vertical theta–theta goniometer having a range of 0°–160° 2θ. The Cu K-alpha-1 radiation was used, whereas nickel metal was used as a beta filter. The particle size of silver nanoparticles was determined by using Debye–Scherrer's equation. Particle Size (D) = $(0.9 \times \lambda)/(\beta \cos\theta)$, where λ is the wavelength (Cu K-alpha = 1.54), β is the full width half- maximum (FWHM) of the peak, θ is diffraction angle [29].

Fourier Transform Infrared (FTIR) Spectroscopy

Two-milligram AgNPs were mixed with 200 mg potassium bromide and pressed into a pellet. The pellet was placed into the sample holder and analyzed using Perkin Elmer - FTIR spectrophotometer (Spectrum 2, USA). The spectra were collected at 28 °C between 4000 and 400 cm^{-1} at a resolution of 4 cm^{-1}. The spectra of $AgNO_3$ with KBr served as a control.

Determination of particle size and zeta potential

The particle size and zeta potential of AgNPs were measured by using Zeta sizer (Malvern, UK). Water was used as the dispersion medium. The refractive index of 1.3, a dielectric constant of 78.5, a viscosity of 0.8 (cP) and temperature of 25 °C were applied and total of 12 zeta runs were analyzed.

Antifungal Activity of AgNPs

The antifungal activity of AgNPs was investigated as per the agar well diffusion method described by Sharma et al. [29] with slight modifications. In brief, 1 mL spore (10^5 mL^{-1}) suspension of phytopathogens (*F. verticillioides, R. solani, U. maydis, S. sclerotiorum, C. dematium* and *C. circinans*) was spread plated on the dry surface of PDA. The wells (∼ 6 mm) were created by using cork-borer and filled with 20 µL solution of different concentrations of AgNPs (20, 60 and 100 µg per well). The plates were kept at 4 °C for radial diffusion. The plates were observed for growth clearance around the wells after incubation at 30 °C for 48–72 h. Nystatin (100 µg/well) was used as a positive control. The zone of clearance was recorded in millimeters (mm).

Investigation on the Mechanism of Antifungal Action of AgNPs

Based on the highest sensitivity to AgNPs, *F. verticillioides* was selected to study the mechanism of antifungal action of AgNPs.

Effect of AgNPs on Conidial Germination and Mycelial Morphology

The mycelial plugs (5 mm diameter) of 24 h old *F. verticillioides* were each inoculated separately in 50 mL potato dextrose broth (PDB) supplemented with 20, 60 and 100 µg mL^{-1} of AgNPs. The culture flasks were incubated at 30 °C for up to 12 h. At the interval of 2, 4, 6, 8, 10, and 12 h, the samples were withdrawn and observed under a compound microscope for the conidia germination. The growth without AgNPs served as a control. The germination rate (%) was calculated according to Hassouni et al. [30].

The SEM analysis was performed to investigate morphological changes after 12 h of incubation [31]. The samples were fixed by using 2.5% (v/v) glutaraldehyde for 2–4 h. After fixation, samples were treated with increasing ethanol levels (30 to 70%, v/v for 15 min and 80 to 100%, v/v for 20 min, respectively). Then samples were subjected to CO_2 drying using aqueous acetone (25, 50, 75 and 100%, v/v) as an intermediate fluid. The dried samples were visualized and imaged by FE-SEM. Lysozyme treated (100 µg mL^{-1}) mycelia of *F. verticillioides* served as a positive control.

Effect of AgNPs on Cell Membrane Permeability

24 h old mycelial plugs (5 mm diameter) were each separately inoculated into 100 mL of PDB. The flasks were incubated on a rotary shaker (120 rpm) for 24 h at 28 °C. After incubation, different concentrations AgNPs (20, 60 and 100 µg mL^{-1}) were added and kept for an additional 24 h. Thereafter, mycelia were collected by vacuum filtration for 20 min and washed twice with sterile distilled water. 0.5 g of mycelia were placed in 20 mL of double distilled water and electrical conductance was measured at time intervals of 0, 5, 10, 20, 40, 60, 80, 100, 120, 140, 160, and 180 min by a conductivity meter (Hanna, USA). The changes in electrical conductivity of distilled water indicated the leaching of cell contents through the membrane [32]. After 180 min, the mycelia were boiled for 5 min, and the final conductivity was measured. The relative conductivity of mycelia was calculated as,

$$\text{Relative conductivity } (\%) = \text{Conductivity}/\text{Final Conductivity} \times 100.$$

Histochemical detection of cell membrane permeability

The effect on cell membrane permeability was determined using a fluorescent probe (propidium iodide, PI) which binds to nucleic acids if the membrane permeability is

compromised [33]. Different concentrations of AgNPs (0, 20, 60 and 100 µg mL^{-1}) were used to treat the fresh mycelia of *F. verticillioides* and incubated for 24 h at 28 °C on a rotary shaker (120 rpm). The mycelia were then separated by centrifugation at 6000×*g* and incubated in 2 mM of PI solution (prepared according to [34]) for 20 min. After incubation, cells were washed thrice with distilled water and visualization (excitation 535 nm) under a fluorescence microscope (ECLIPSE, TE 2000-S, Nikon, China).

Determination of Ergosterol Content of Cell Membrane

Total intracellular sterol was extracted and determined as per the method described by Arthington-Skaggs et al. [35] with slight modifications. Mycelial plugs (5 mm diameter) of 24 h old *F. verticillioides* were each separately inoculated in 50 mL PDB supplemented with 0, 20, 60 and 100 µg mL^{-1} AgNPs. The lysozyme and fluconazole (each 100 µg mL^{-1}) served as positive controls. After incubation at 28 °C for 24 h, the biomass was collected by centrifugation at 6000×*g* for 5 min and washed with sterile distilled water. The weight of biomass was recorded. Then, 3 mL of 25% (w/v) alcoholic-KOH solution (25 g KOH in 35 mL of distilled water, volume made up to 100 mL with absolute ethanol) was added and vortexed for 1 min. The cell suspensions were incubated in 85 °C water bath for 1 h in sterile borosilicate screw cap bottles. After incubation, the samples were cooled to room temperature. The sterol from the samples was extracted by aqueous η-heptane in 1:3 proportion followed by vigorous vortex mixing for 3 min. The heptane layer was removed and stored at 22 °C. Before analysis, 20 µL aliquot of sterol extract was diluted fivefold in absolute ethanol and scanned between 220 and 300 nm using UV–Vis spectrophotometer. The ergosterol content was calculated as a percentage of the wet weight of cell by the following equation,

$$\% \text{ ergosterol } = [(A_{281.5}/290) \times F]/\text{pellet weight}$$

$$\%24(28) \text{ DHE} = [(A_{230.0}/518) \times F]/\text{pellet weight}$$

where, *F* is the factor for dilution in ethanol and 290 and 518 are the *E* values (in percentages per centimeter) determined for crystalline ergosterol and 24(28) DHE, respectively. From percent content, the percent reduction in ergosterol synthesis was calculated.

Statistical Analysis

Statistical analyses were performed using GraphPad Prism (USA). All experiments were performed in triplicates. The differences among means were determined using One-Way ANOVA and multiple comparisons at significance and confidence levels of 0.05 (95% confidence interval) was determined. The *p* value of < 0.05 was considered significant.

Results

Screening of Haloalkaliphilic *Streptomyces* spp. for Biological Synthesis of AgNPs

The culture supernatants of *Streptomyces* spp. designated as VL 4, VL 5, VL 18, VL 50, VL 61 and VL J2, showed the color change from yellow to brown when incubated along with $AgNO_3$. Of these strains, culture supernatant of *Streptomyces* spp. VL J2 showed the peak with maximum absorbance at 400–430 nm in spectrophotometric analysis (Fig. 1a).

Streptomyces spp. VL J2 supernatant when incubated along with 1 mM solution of $AgNO_3$ showed the gradual color change from yellow to dark brown (Fig. 1b inset). The UV visible spectra showed a progressively stronger peak at 430 nm (λ_{max}) as a function of time (24, 48 and 72 h) (Fig. 1b).

Characterization of AgNPs

Scanning and Transmission Electron Microscopy

SEM and TEM images of AgNPs showed the spherical and polydisperse particles with an average diameter of 16.4 ± 2.2 nm (Fig. 2a, b, e). Besides this, the disc structures were noticed along with larger and small spherical particles (Fig. 2a). The HR-TEM image of a single nanoparticle showed the lattice spacing (Fig. 2c). The bright circular concentric spots in selected area electron diffraction (SAED) pattern indicated the crystallinity of biologically synthesized AgNPs (Fig. 2d). Moreover, the EDX analysis of AgNPs showed the presence of silver ions (Fig. 2f).

XRD Analysis

The XRD spectrum of AgNPs showed four distinct sharp diffraction peaks at 32.27°, 45.47°, 66.28° and 76.84° on 2θ scale. Besides this, few other peaks were also noticed near to the characteristic peaks (Fig. 3a). The average crystalline size D of the AgNPs was estimated from diffractogram by using Debye–Scherrer formula,

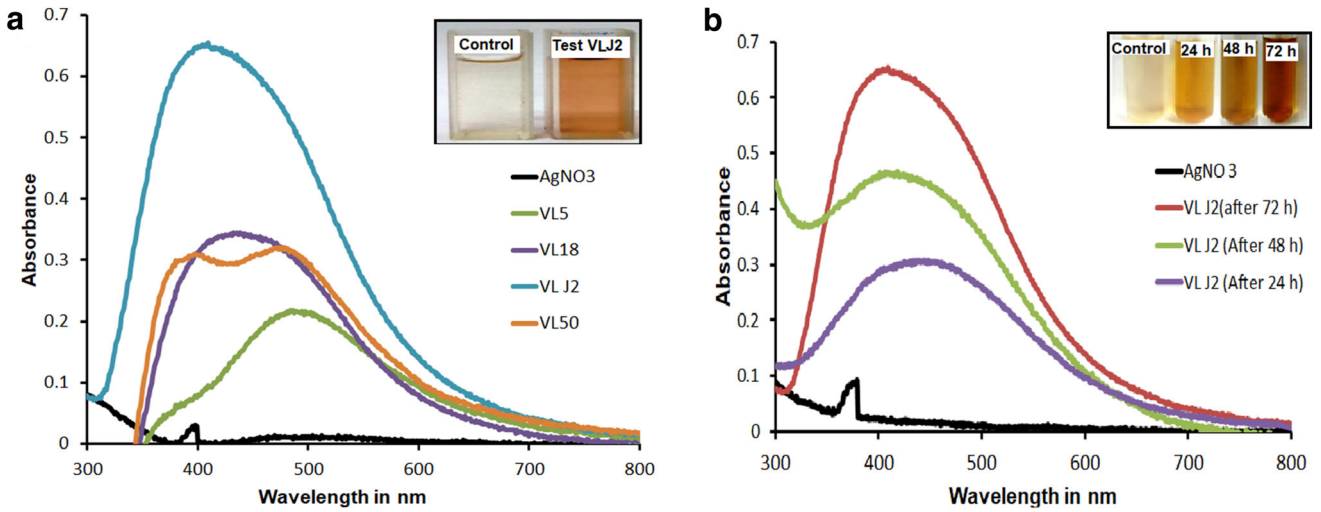

Fig. 1 **a** Screening of *Streptomyces* spp. for synthesis of silver nanoparticles; **b** UV–visible spectroscopic analysis of biologically synthesized AgNPs by *Streptomyces* spp. VL J2

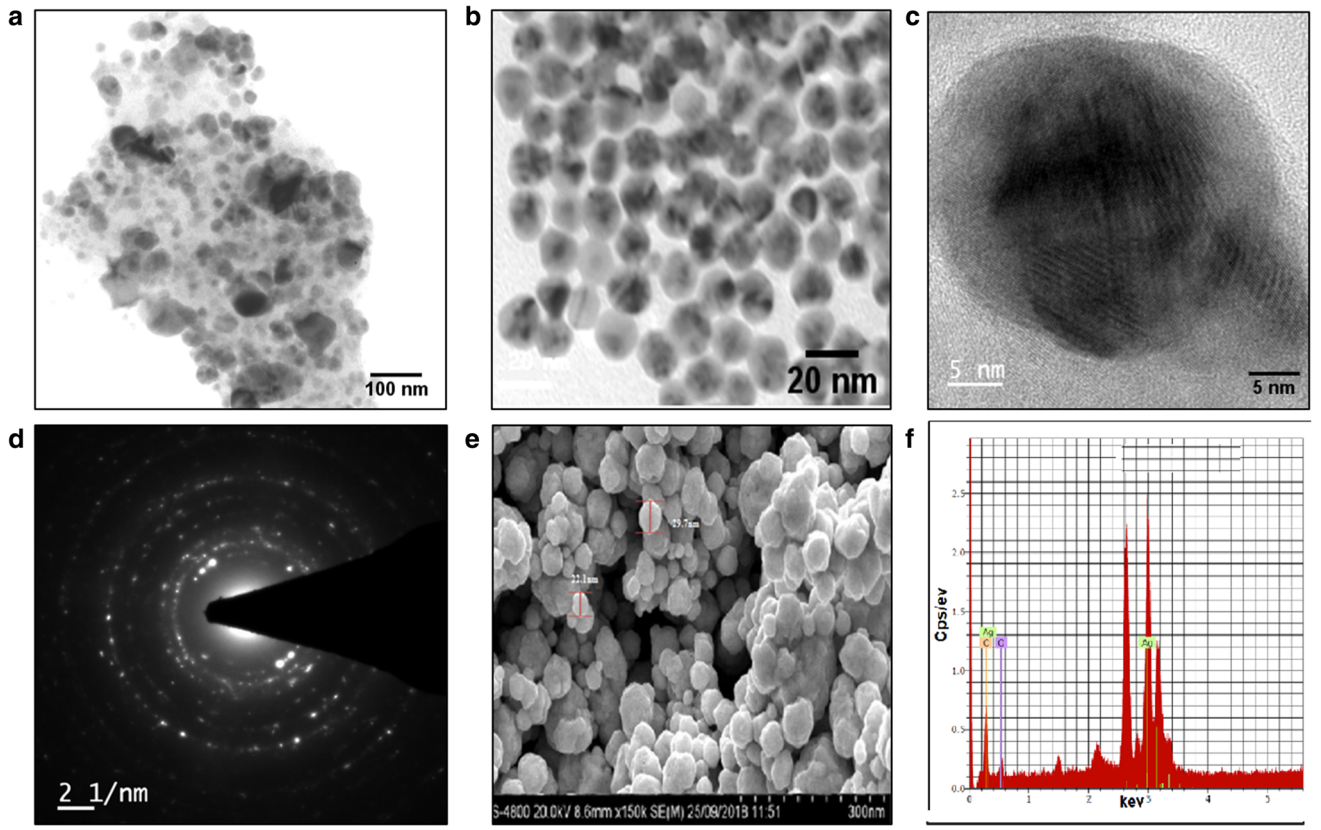

Fig. 2 Electron microscopy images of biologically synthesized AgNPs. **a**, **b** TEM at different scale; **c** HR-TEM; **d** SAED pattern; **e** SEM image; **f** EDX of AgNPs

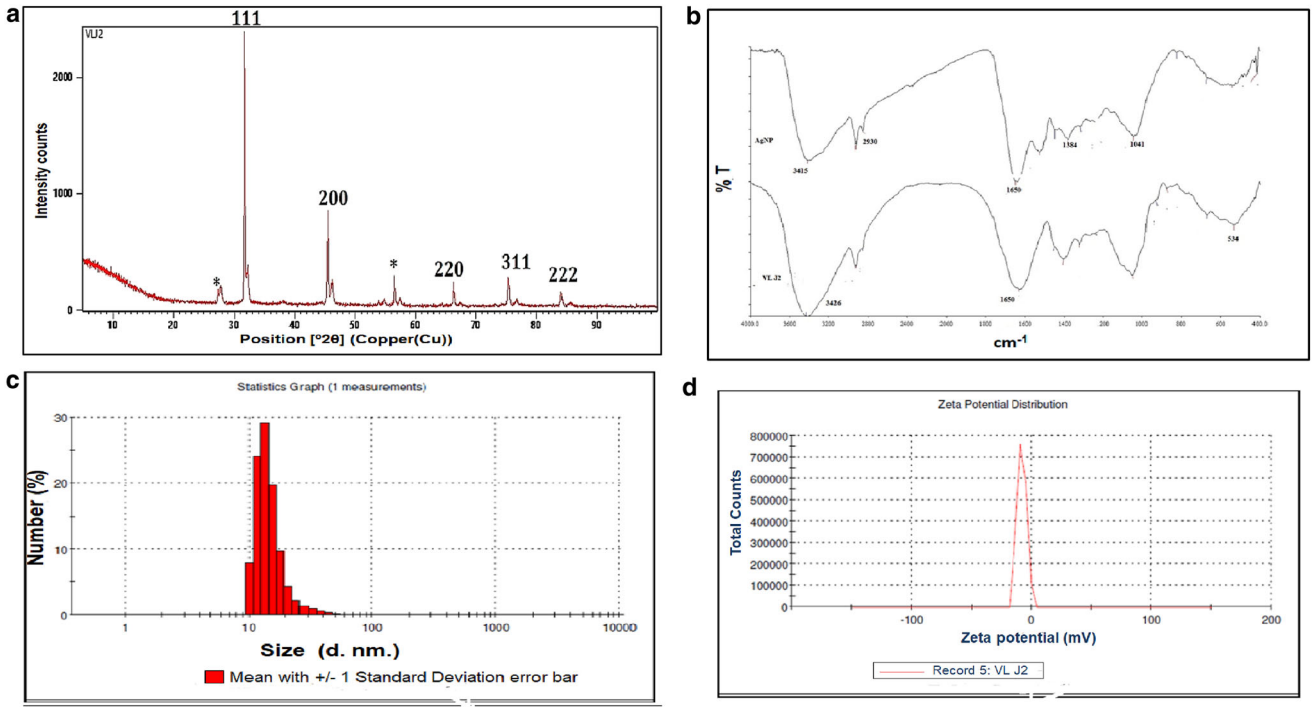

Fig. 3 **a** XRD spectra; **b** FTIR spectra; **c** Particle size distribution; **d** Zeta potential distribution of biologically synthesized AgNPs from *Streptomyces* spp. VL J2

$$D = 0.9\lambda/\beta \text{ Cos } \theta,$$

where λ is the wavelength of X-rays used for diffraction and β is full width at half maximum (FWHM) of a peak. The calculated average crystalline size of the silver nanoparticles was estimated to be 22.05 nm (Table 1).

FTIR Analysis

FTIR analysis of AgNPs showed total five absorbance bands at 3415 (O–H stretching), 2923 (C–H stretching), 1650 (C=O stretching), 1384 (–C–N stretching) and 1041 (C–O stretching) cm^{-1} (Fig. 3b). Due to the reducing and capping properties of culture supernatant, a marginal shift in the peak position of spectra was observed.

Particle Size and Zeta Potential Analysis

The particle size analyzer showed that biologically synthesized AgNPs had an average diameter of 119.7 nm (Fig. 3c). The zeta potential of AgNPs was − 8.12 ± 3.87 mV (Fig. 3d).

Antifungal Activity of AgNPs

AgNPs at the concentration of 20, 40, 60 and 100 µg per well significantly inhibited the growth of *F. verticillioides* and *U. maydis*. The zone of inhibitions recorded against *F. verticillioides* (20 µg: 9.9 ± 0.2; 40 µg: 10.7 ± 0.4; 60 µg: 12.2 ± 0.8; 100 µg: 18 ± 0.2 mm; nystatin 100 µg: 11 ± 0.4 mm) were significantly ($p < 0.05$) higher as compared with *U. maydis* (20 µg: 2.1 ± 0.1; 40 µg: 9.1 ± 0.7; 60 µg: 10.5 ± 0.6; 100 µg: 11.5 ± 0.5 mm; nystatin 100 µg: 7.3 ± 0.1 mm). No activity was detected against *R. solani*, *S. sclerotiorum*, *C. dematium* and *C. circinans*.

Investigation on the Mechanism of Antifungal Action of AgNPs

Effect of AgNPs on Conidial Germination and Mycelial Morphology of *F. verticillioides*

After 12 h of incubation, the germination of *F. verticillioides* conidia was significantly ($p < 0.05$) decreased in presence of 100 µg mL^{-1} AgNPs as compared to control (no AgNPs) and 20 and 60 µg mL^{-1} AgNPs. The percent germination inhibition was calculated to be 55% in presence of 100 µg mL^{-1} AgNPs (Fig. 4). The delayed conidia germination was noticed in the presence of higher levels of AgNPs (Fig. 4).

SEM analysis revealed the morphological deformations and damages in hyphae treated with different concentrations of AgNPs (0, 20, 60 and 100 µg mL^{-1}). At 20 µg mL^{-1} concentration, the number of vacuoles with

Table 1 XRD analysis profile of AgNPs synthesized by *Streptomyces* spp. VLJ2

Peak no.	2θ (Degree)	Cos θ	FWHM (Degree)	β (Radian)	Crystalline size D (A°)	Crystalline size D (nm)
1.	32.27	0.946	0.42	0.0062	237.7	23.7
2.	45.47	0.924	0.39	0.0068	222.5	22.2
3.	66.28	0.841	0.52	0.0092	179.2	17.9
4.	76.84	0.783	0.40	0.0096	184.1	18.4
5.	83.98	0.745	0.36	0.0068	276.6	27.6
Avg. crystalline size D					220.00	22.00

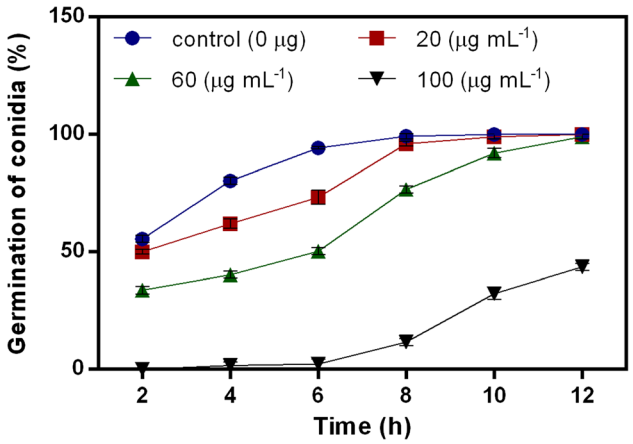

Fig. 4 Effect of AgNPs on conidial germination of *Streptomyces* spp. VL J2

different sizes was detected inside the cells (Fig. 5b). A loss of shape/irregular shrinkage of hyphae was observed at 60 µg mL^{-1} concentration (Fig. 5c) as compared to the control hyphae (Fig. 5a). The hyphae were fragmented when grown in presence of 100 µg mL^{-1} AgNPs (Fig. 5d, e). Lysozyme treatment (100 µg mL^{-1}) indicated the loss of structure (Fig. 5f) as like 100 µg mL^{-1} AgNPs.

Similarly, AgNPs induced damage to the spores increased with increase in its concentration in media. Spores in the control group (without AgNPs) were smooth, with a regular shape (Fig. 6a), while spores treated with 20 and 60 µg mL^{-1} of AgNPs showed irregular shape and shrinkage (Fig. 6b, c). At 100 µg mL^{-1}, spores were damaged (shrinking and lysis) as like in presence of lysozyme (positive control) (Fig. 6d–f).

Effect of AgNPs on Cell Membrane Permeability

There was a significant ($p < 0.05$) increase in the relative conductivity of *F. verticillioides* mycelia when treated with AgNPs (100, 60, and 20 µg mL^{-1}) as compared to control (without AgNPs) (Fig. 7a). About 20% increase in relative conductivity of mycelia was observed at 100 µg mL^{-1} AgNPs as compared to control.

Histochemical Detection of Cell Membrane Permeability

Propidium iodide (PI) is a nucleic acid-binding fluorescent probe that penetrates the compromised cell membrane and shows intense red fluorescence [36]. The AgNPs (20, 60, and 100 µg mL^{-1}) treated *F. verticillioides* hyphae showed extensive red fluorescence at 535 nm as compared to control (Fig. 7b).

Determination of Ergosterol Content of Cell Membrane

The 42.85 and 17.85% reduction ($p < 0.05$) in ergosterol biosynthesis was observed at 100 and 60 µg mL^{-1} concentration of AgNPs as compared to control (Fig. 7c). In UV–visible spectroscopic analysis, samples treated with AgNPs failed to show the characteristics—four peak curve (ergosterol and late sterol 24(28) DHE) between 240 and 300 nm as compared to control (no AgNPs) (Fig. 7d). Besides this, the absorbance intensity of four peaked curves decreased with increasing AgNP levels. A flat line was observed at 100 µg mL^{-1} AgNPs and thymol (positive control). Moreover, lysozyme and fluconazole (100 µg mL^{-1} each) showed no reduction in characteristics of four peaked curves (Fig. 7d).

Discussion

This study presents the biogenic synthesis and characterization of silver nanoparticles using haloalkaliphilc *Streptomyces* spp. and its mechanism-based antifungal activity against *Fusarium verticillioides*. The biological synthesis of silver nanoparticles by bacteria, fungi and plants is already reported by many workers [30, 37, 38]. However, there are very few reports on silver nanoparticle synthesis by haloalkaliphilic *Streptomyces* spp. Recently, Wypij et al. [18] reported biogenic silver nanoparticles synthesis by *S. xinghiensis* OF1 strain. The biogenic synthesis of AgNPs using the *Streptomyces* spp. have significant advantages in comparison with the physical and chemical methods.

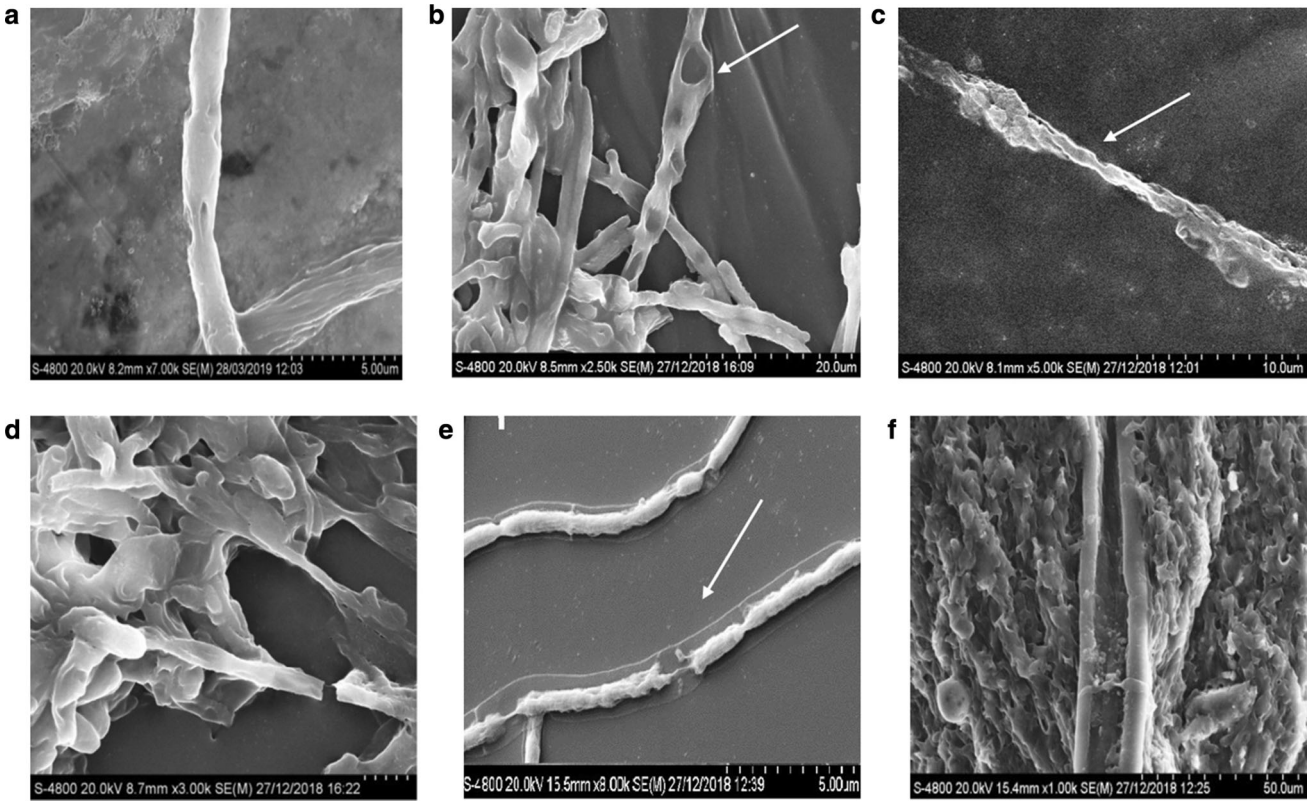

Fig. 5 Effect of AgNPs on the hyphal morphology of *F. verticillioides* (NCIM 4947). **a** 0 (control); **b** 20; **c** 60; **d**, and **e** 100 μg mL^{-1} AgNPs; **f** Lysozyme (100 μg mL^{-1})

The strain *Streptomyces* spp. VL J2 showed the maximum production of silver nanoparticles may be due to the reduction of silver salt by secondary metabolites. The compounds which contribute the reduction and oxidation are still not known, however, *Streptomyces* spp. VL J2 has previously been reported for the production of protease inhibitors [27, 28]. Broadening of SPR absorption bands with absorption tail in the longer wavelengths could be due to shape, size distribution and aggregation of particles [11]. It should be pointed out here that spherical silver nanoparticles are known to show absorption bands in the range of 400-450 nm in the UV- Visible spectroscopy [12, 13, 17, 18, 39]. Further characterization of AgNPs using SEM and TEM indicated the production of spherical shaped nanoparticles with average diameter of 16.4 ± 2.2 nm. These results are in agreement that AgNPs produced by *Streptomyces* strains are spherical with average size 5-20 nm [16, 18]. The bright circular concentric spots of different lattice planes observed in selected area electron diffraction (SAED) study confirmed the crystalline nature of biologically synthesized AgNPs. In EDX analysis, the absorption peak at 3 keV is typical for metallic silver nanoparticles [40]. The Cu peak observed was due to the copper grid on which the sample was coated. Moreover, the results of EDX analysis indicate that the AgNPs synthesized from *Streptomyces* spp. VL J2 were pure and crystalline.

In XRD studies, the distinct diffraction peaks observed at 32.27°, 45.47°, 66.28° and 76.84° corresponded well to (111), (200), (220) and (311) planes of crystalline silver of JCPDS file (No. 04-0783). Few unassigned peaks observed were may be due to the capping agent stabilizing the nanoparticles [17, 35]. The calculated average crystalline size of the silver nanoparticles was 22.05 nm. Moreover, XRD thus confirmed that the resultant particles in the sample are silver nanoparticles having face-centered cubic crystal structure, which corroborates well with the size determined by SEM and TEM analyses. The FTIR analysis showed strong bands at 1650 and 1384 cm^{-1} mainly due to amide group and -C-N stretching vibrations of proteins suggesting the protein present in a culture supernatant of VL J2, which could act as a capping agent for stabilizing the AgNPs. Karthik et al. [17] and Omran et al. [41] earlier showed that proteins may act as a reducing and capping agent for the synthesis of silver nanoparticles and they may also increase the stability of synthesized AgNPs.

The average diameter of 119.7 nm determined by particle size analyzer could be due to the aggregation of particles. The biogenically synthesized AgNPs were found to be negatively charged (− 8.12 mV) which may offer

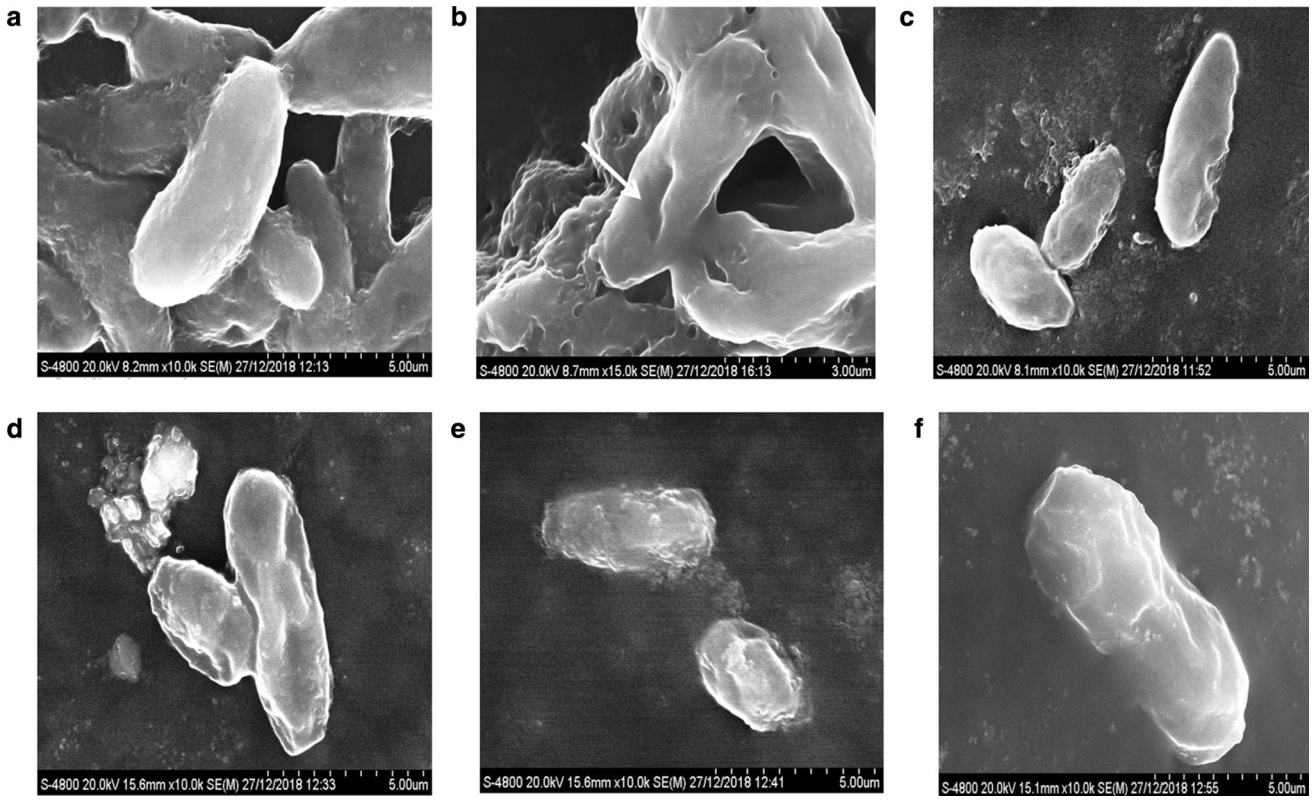

Fig. 6 Effect of AgNPs on the spore morphology of *F. verticillioides* (NCIM 4947). **a** 0 (control); **b** 20; **c** 60; **d**, and **e** 100 μg mL^{-1} AgNPs; **f** Lysozyme (100 μg mL^{-1})

high stability to the nanoparticles. Prakasham et al. [42] reported − 8.5 mV zeta potential for the AgNPs synthesized by *S. albidoflavus*. Recently, *S. xinghaiensis* OF1 has been shown to produce highly stable negatively charged biogenic AgNPs with -15.7 mV zeta potential [18].

Of the fungal pathogens tested, *F. verticillioides* was most sensitive to inhibition followed by *U. maydis* at 20 μg concentration of AgNPs, as compared to the standard (Nystatin at 100 μg) whereas, no inhibition was observed against *R. solani, S. sclerotiorum, C. dematium* and *C. circinans*. Balashanmugama et al. [43] reported the maximum antifungal activity of phyto-synthesized AgNPs against *R. solani*, *F. oxysporum* and *Curvularia sp.* Based on sensitivity to AgNPs, *F. verticillioides* was selected for the study of biochemical mechanism for antifungal activity of AgNPs.

This study suggested that the presence of AgNPs in culture media delay the process of conidia germination. Earlier, Gao et al. [32] reported the delay of germination in *Fusarium graminearum* treated with different concentrations of thymol. Vacuoles play important role in filamentous fungi in response to osmotic stress [44]. In the present study, as evident in SEM, a considerable increase in vacuole number in hyphae of *F. verticillioides* was observed which might be due to osmotic stress induced by AgNPs. Amro et al. [45] suggested that AgNPs can easily pass through the cell wall due to their small size and accumulate in the cell membrane to form irregular- shaped pits. Accumulation of AgNPs affects the respiratory chain and membrane permeability which lead to lysis of cell [46]. Therefore, the possible mechanisms behind the irregular shape and lysis of spores observed in the present study might be due to the accumulation of small size biogenic AgNPs in the membrane. Deformities in mycelial growth and shape of hyphal walls of *Colletotrichum gloeosporioides* treated with silver nanoparticles have been reported [47] and our results are in agreement with them. Also, there are many reports on the delay of mycelial growth of different phytopathogenic fungi when treated with biogenic silver nanoparticles [48–50]. An increase in relative conductivity could be an indication of electrolyte leakage due to the increase in cell membrane permeability of *F. verticillioides*. Recently, it was observed that AgNPs mediated morphological changes in membrane structure may disrupt membrane permeability and, finally leaded leakage of ions, bound proteins and enzymes [51]. Our results appear to be in line with these findings and explain the probable mechanism of antifungal activity of AgNPs against *F. verticillioides.* The increase in red fluorescence as a function of AgNPs treatment suggested that AgNPs could

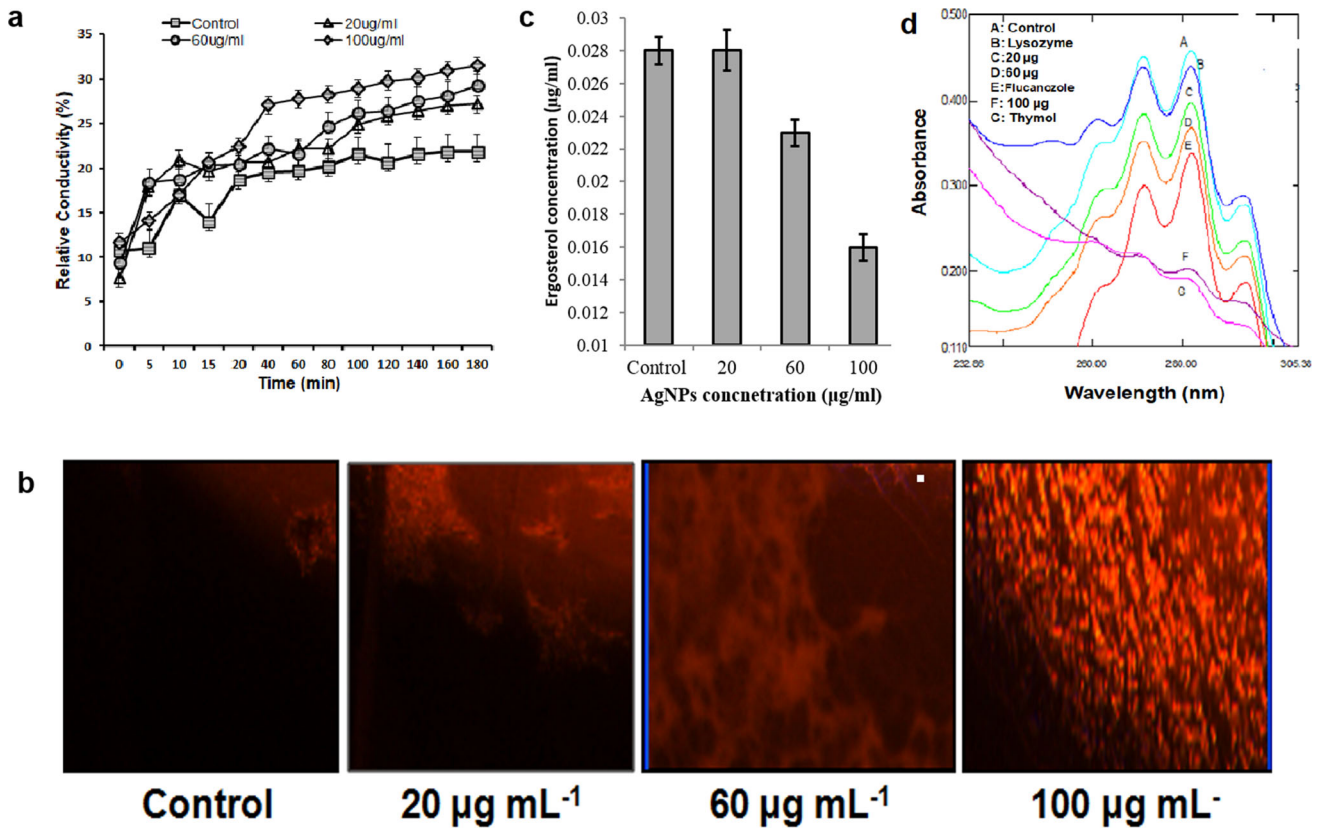

Fig. 7 Effect of AgNPs on, **a** relative conductivity; **b** hyphae membrane (stained with propidium iodide); **c** ergosterol content; and **d** sterol profile (UV-Spectrophotometric) of *F. verticillioides*

induce the cell membrane injury or increase membrane permeability, which corroborates well with the previously discussed results. Similarly, silver NPs mediated cell membrane damage and an increase in cell membrane permeability of *Vibrio parahaemolyticus* and *Staphylococcus aureus* was reported by Du et al. [52].

Ergosterol is the prime constituent of cell membranes of fungi, which serves as a bioregulator of membrane fluidity and regulate the physiological functions of the membrane [10]. There was no report on inhibition of AgNPs mediated ergosterol biosynthesis. Recently Xu [53] reported that polyene antibiotics selectively bind with fungal ergosterol which results in cellular leakage and damage to the membrane structure. Similarly, plant-derived metabolites like flucanozole and thymol are known to significantly induced impairment of ergosterol biosynthesis in *Candida spp.* [32, 35] Furthermore, a decrease in ergosterol level in hyphae of fungus *F. oxysporum* was observed when treated with the culture supernatant of *Streptomyces bikiniensis* HD-087 [10]. As per our knowledge, this is the first report on the AgNPs mediated inhibition of ergosterol biosynthesis of the fungal cell membranes. Collectively our results suggested strong antifungal activity of biogenically synthesized AgNPs against one of the important plant pathogenic fungi, *F. verticillioides.* The probable mode of action of AgNPs could involve severe damage to the cell membrane resulting in mycelial breakage, shrinkage of conidia, increase in relative conductivity and membrane permeability and decrease in ergosterol content of the membrane.

In conclusion, haloalkaliphilic *Streptomyces* spp. has a potential for reliable, eco-friendly, and simple green synthesis of AgNPs. The synthesized AgNPs showed excellent antifungal activity against plant pathogenic fungi. SEM, histo- and biochemical approaches used to investigate the mode of action of AgNPs suggested that antifungal activity could be due to inhibition of ergosterol biosynthesis leading to severe damage to the cell membrane. It would be interesting to study the action of AgNPs on the biosynthetic pathway of ergosterol synthesis at the molecular level (to check the effect on the expression of genes responsible for ergosterol biosynthesis). In our opinion, the synthesized AgNPs, either alone or in suitable combination, could prove to be a good alternative strategy for controlling phytopathogen.

Acknowledgements KRM acknowledges SERB (Science and Engineering Research Board, Govt. of India) for providing N-PDF (File No. N-PDF/2017/0000115 dated 6/10/2017). Authors are thankful to

Dr. Bhardwaj, Jain Irrigation System Ltd., Jalgaon, India for kind help with fluorescent microscopy. Authors are also grateful to University Grants Commission, New Delhi and Department of Science and Technology, Govt. of India for making the research facilities available under the UGC-SAP and DST-FIST programs sanctioned at both places, the School of Life Sciences and the University Institute of Chemical Technology, KBCNMU, Jalgaon.

References

1. U. Basavaraj, N. Praveenkumar, S. Sabiha, S. Rupali, and B. Samprita (2012). *Int. J. Pharm. Bio Sci.* **2**, 10–14.
2. J. Ahire and L. Dicks (2016). *Curr. Microbiol.* **73**, 236–241.
3. F. Chen, M. Ding, X. Wang, and L. Shao (2004). *Biomaterials* **25**, 723–727.
4. S. Aminabad, M. Farshbaf, and A. Akbarzadeh (2019). *Cell Biochem. Biophys.* **77**, 123–137.
5. T. Wang, L. Yang, B. Zhang, and J. Liu (2010). *Colloid Surf. B* **80**, 94–102.
6. D. Muhammad and R. Rida (2017). *Anal. Lett.* **50**, 50–62.
7. F. Gholami, H. Mosmeri, M. Shavandi, M. Dastgheib, and A. Amoozegar (2019). *Sci. Total Environ.* **655**, 633–640.
8. R. Rao, U. Kulkarni, J. Thomas, and P. Edwards (2000). *Chem. Soc. Rev.* **29**, 27–35.
9. M. Rai, A. Yadav, and A. Gade (2009). *Biotechnol. Adv.* **27**, 76–83.
10. S. Zhao, M. Du, and Y. Tian (2012). *World J. Microbiol. Biotechnol.* **28**, 2919–2927.
11. A. Ahmad, P. Mukherjee, S. Senapati, D. Mandal, I. Khan, R. Kumar, and M. Sastry (2003). *Colloids Surf. B* **28**, 313–318.
12. N. Kharat and D. Mendhulkar (2016). *Mat. Sci. Eng. C* **62**, 719–724.
13. P. Manivasagan, V. Jayachandran, S. Kalimuthu, S. Kannan, and K. Se-Kwon (2013). *Biomed. Res. Int*. 1–9.
14. S. Kim, K. Houng, L. Hyun, and J. Kye (1991). *J. Microbiol. Biotechnol.* **1**, 288–292.
15. Y. Tsibakhashvili, I. Kirkesali, T. Pataraya, A. Gurielidze, L. Kalabegishvili, N. Gvarjaladze, et al. (2011). *Adv. Sci. Lett.* **4**, 3408–3417.
16. S. Sadhasivam, P. Shanmugam, and K. Yun (2010). *Colloids Surf. B* **81**, 358–362.
17. L. Karthik, G. Kumar, V. Kirthi, A. Rahuman, and B. Rao (2014). *Bioproc. Biosyst. Eng.* **37**, 261–267.
18. M. Wypij, J. Czarnecka, M. Świecimska, H. Dahm, M. Rai, and P. Golinska (2018). *World J. Microbiol. Biotechnol.* **34**, 23 (1–13).
19. G. Agrios *Plant Pathology*, 5th ed (Elsevier Academic Press, San Diego, 2005).
20. A. Dhekney, T. Li, M. Van Aman, M. Dutt, J. Tattersall, T. Kelley, and J. Gray (2005). *Fruit Crops Tropical Species* **738**, 743–748.
21. N. Krishnan, B. Velramar, and K. Velu (2019). *Pest Biochem. Physiol.* **155**, 101–107.
22. W. Bacon, E. Yates, M. Hinton, and F. Meredith (2001). *Environ. Health Perspect* **109**, 325–332.
23. J. Ahire, D. Neveling, and L. Dicks (2015). *Curr. Microbiol.* **71**, 24–30.
24. A. Sidhu, S. Ghatelwal, K. Gumber, and A. Bala (2017). *Appl. Nanosci.* **7**, 617–623.
25. A. Petica, S. Gavriliu, M. Lungu, N. Buruntea, and C. Panzaru (2008). *Mater Sci Eng B* **152**, 22–27.
26. W. Kim, S. Kim, K. Lamsal, J. Kim, B. Kim, M. Jung, and S. Lee (2009). *J. Microbiol. Biotechnol.* **19**, 760–764.
27. K. Marathe, S. Kasar, A. Chaudhari, and V. Maheshwari (2016). *Proc. Biochem.* **51**, 1650–1663.
28. K. Marathe, A. Chaudhari, K. Kamalaja, and V. Maheshwari (2015). *Biocatal. Agric. Biotechnol.* **5**, 58–68.
29. R. Sharma, D. Acharya, S. Moghe, B. Shrivastava, M. Gangrade, T. Shripathi, and V. Ganesan (2014). *Mat. Sci. Semicon. Proc.* **23**, 42–49.
30. M. Elamawi, E. Al-Harbi, and A. Hendi (2018). *Egypt J. Biol. Pest Co.* **28**, 28.
31. H. Hassouni, I. Alaoui, K. Lamrani, G. Perraud, C. Augur, and S. Roussos (2007). *Micol. Aplicada Int.* **19**, 7–14.
32. T. Gao, H. Zhou, W. Zhou, L. Hu, J. Chen, and Z. Shi (2016). *Molecules* **21**, 770.
33. Y. Duan, C. Ge, S. Liu, C. Chen, and M. Zhou (2013). *Pest Biochem. Physiol.* **106**, 61–67.
34. H. Firstencel, M. Butt, and I. Carruther (1990). *J Invertebr Pathol* **55**, 258–264.
35. A. Arthington-Skaggs, H. Jradi, T. Desai, and J. Morrison (1999). *J. Clin. Microbiol.* **37**, 3332–3337.
36. A. Bose, H. Keharia, and P. Deshpande (2013). *Chin. Phys. Lett.* **30**, 128103.
37. X. Wei, M. Luo, W. Li, L. Yang, X. Liang, et al. (2012). *Bioresour Technol* **103**, 273–278.
38. S. Pirtarighat, M. Ghannadnia, and S. Baghshahi (2019). *J. Nanostruct. Chem.* **9**, 1–9.
39. X. Zhao, L. Yan, X. Xu, H. Zhao, Y. Lu, Y. Wang, et al. (2019). *Appl. Microbiol. Biotechnol.* **103**, 1–4.
40. S. Eppler, G. Rupprechter, A. Anderson, and A. Somorjai (2000). *J Phys Chem B* **104**, 7286–7292.
41. A. Omran, N. Nassar, A. Younis, A. Fatthallah, A. Hamdy, H. Shatoury, and N. El- Gendy (2018). *J. Appl. Microbiol.* **126**, 138-154.
42. S. Prakasham, K. Buddana, K. Yannam, and S. Guntuku (2012). *J. Micobiol. Biotechnol.* **22**, 614–621.
43. P. Balashanmugam, D. Balakumaran, R. Murugan, K. Dhanapal, and T. Kalaichelvan (2016). *Microbiol. Res.* **192**, 52–64.
44. A. Richards, V. Veses, and A. Gow (2010). *Fung Biol. Rev.* **24**, 93–105.
45. A. Amro, P. Kotra, K. Wadu-Mesthrige, A. Bulychev, S. Mobashery, and Y. Liu (2000). *Langmuir* **16**, 2789–2796.
46. L. Elechiguerra, L. Burt, R. Morones, A. Camacho-Bragado, X. Gao, H. Lara, and J. Yacaman (2005). *J. Nanobiotechnol*. 3–6.
47. K. Lamsal, W. Kim, H. Jung, S. Kim, S. Kim, and S. Lee (2011). *Mycobiol* **39**, 194–199.
48. A. Aguilar-Méndez, E. San Martín-Martínez, L. Ortega-Arroyo, G. Cobián-Portillo, and E. Sánchez-Espíndola (2011). *J. Nanopart. Res.* **13**, 2525–2532.
49. V. Mahdizadeh, N. Safaie, and F. Khelghatibana (2015). *J. Crop. Prot.* **4**, 291–300.
50. M. Khatami, N. Zafarnia, H. Bami, I. Sharifi, and H. Singh (2018). *J. Mycol. Med.* **28**, 37–644.
51. A. Roy, O. Bulut, K. Mandal, and D. Yilmaz (2019). *RSC Adv.* **9**, 2673–2702.
52. J. Du, Z. Hu, Z. Yu, H. Li, J. Pan, D. Zhao, and Y. Bai (2019). *Mat. Sci. Eng. C* **102**, 247–253.
53. Z. Xu *General Plant Pathology* (Higher Education Press, Beijing, 2009). **(in Chinese)**.